Electronic Supplementary Material (ESI) for Journal of Materials Chemistry A.

Electronic Supporting Information

A Cost-Effective Synthesis of Heteroatom-Doped Porous Carbons as Efficient CO_2 Sorbents

Babak Ashourirad,[a] Pezhman Arab,[a] Timur Islamoglu,[a] Katie Cychosz,[b] Matthias Thommes,[b] and Hani M. El-Kaderi [*a]

[a] Department of Chemistry
Virginia Commonwealth University
Richmond, VA 23284, USA
*E-mail: helkaderi@vcu.edu
Fax: +1 804 828 8599; Tel: +1 804 828 7505

[b] Quantachrome Instruments
1900 Corporate Drive
Boynton Beach, FL 33426, USA

Table S1. Surface area, pore volume and N content of BIDCs synthesized at three different temperatures and KOH/BI=2.

Sample	S_{BET} [$m^2 g^{-1}$]	V_{Total} [$cm^3 g^{-1}$]	N Content [wt%]
BIDC-2-600	895	0.38	14.0
BIDC-2-700	2465	1.34	5.7
BIDC-2-800	3335	1.75	1.5

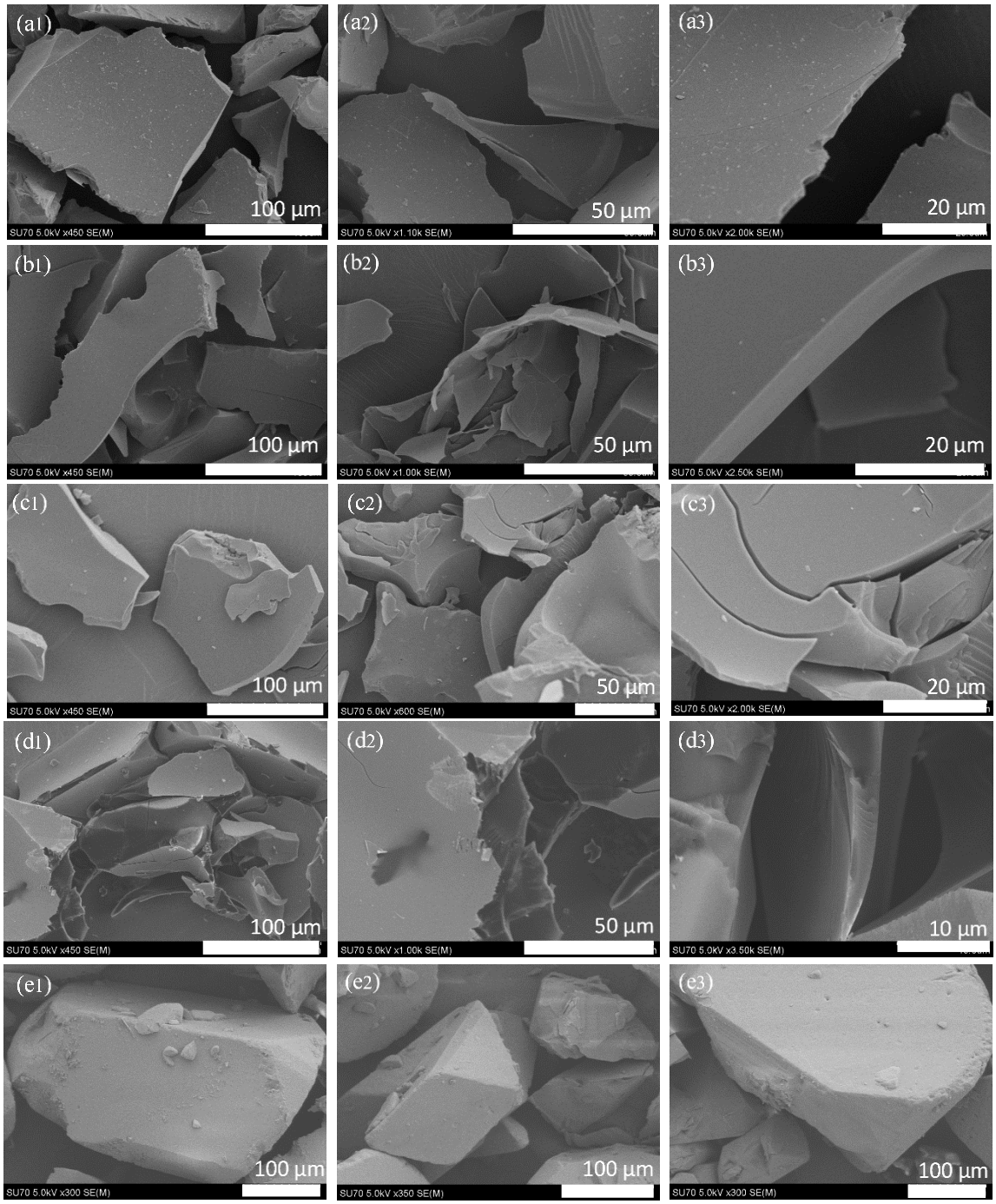

Figure S1. Additional SEM images of BIDCs with different magnifications; a_1-a_3) BIDC-0.5-700, b_1-b_3) BIDC-1-700, c_1-c_3) BIDC-2-700, d_1-d_3) BIDC-3-700, and f_1-f_3) BI.

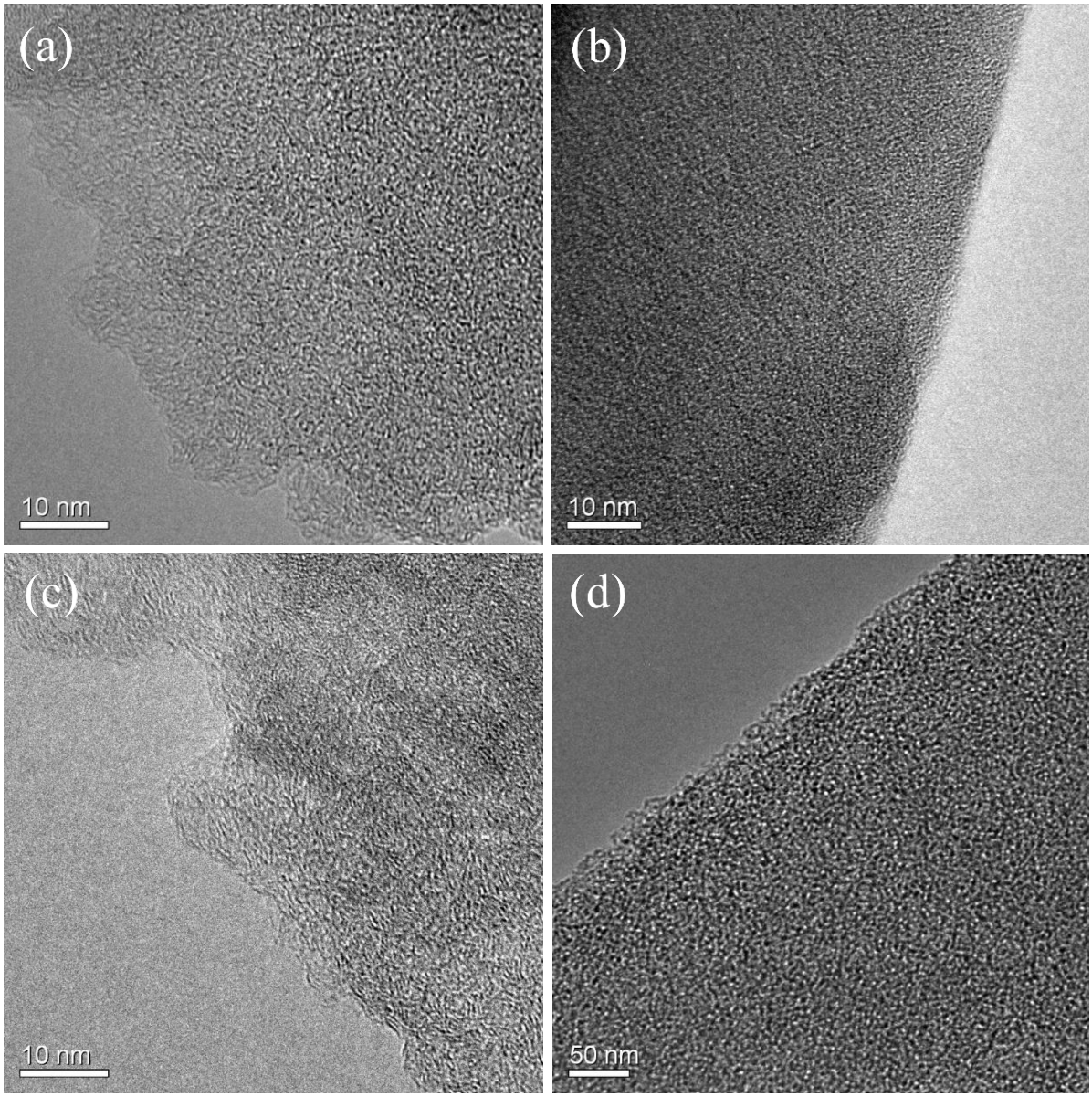

Figure S2. Additional TEM images of BIDCs with different magnifications; a) BIDC-0.5-700, b) BIDC-1-700, c) BIDC-2-700, and d) BIDC-3-700.

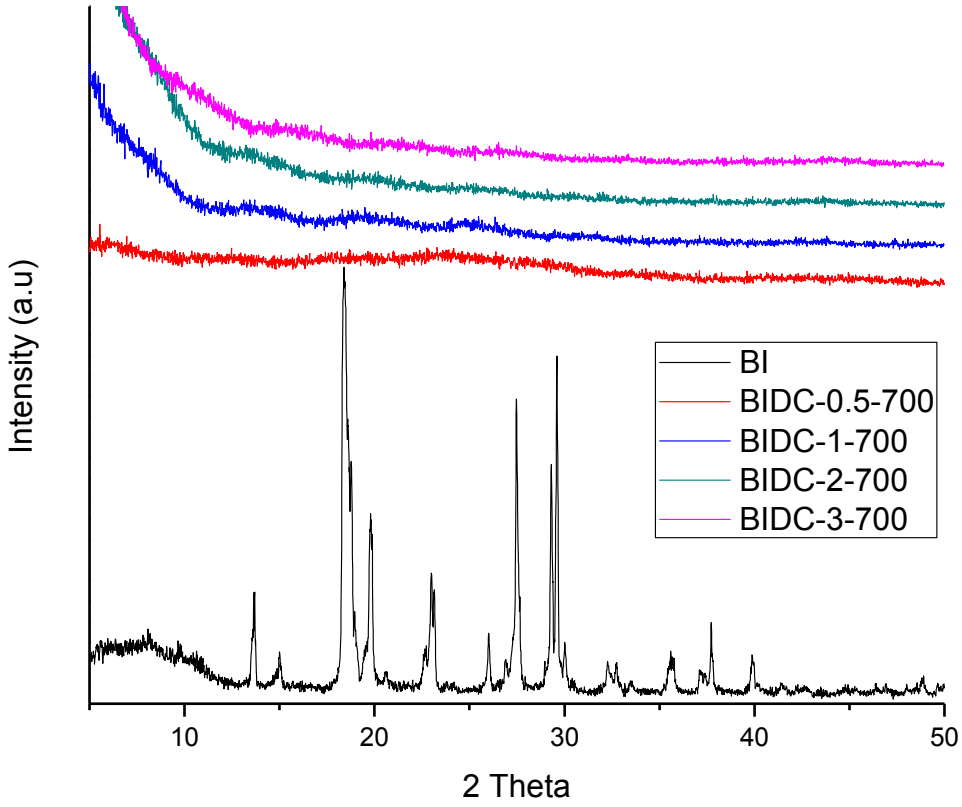

Figure S3. XRD patterns of BIDCs and BI precursor.

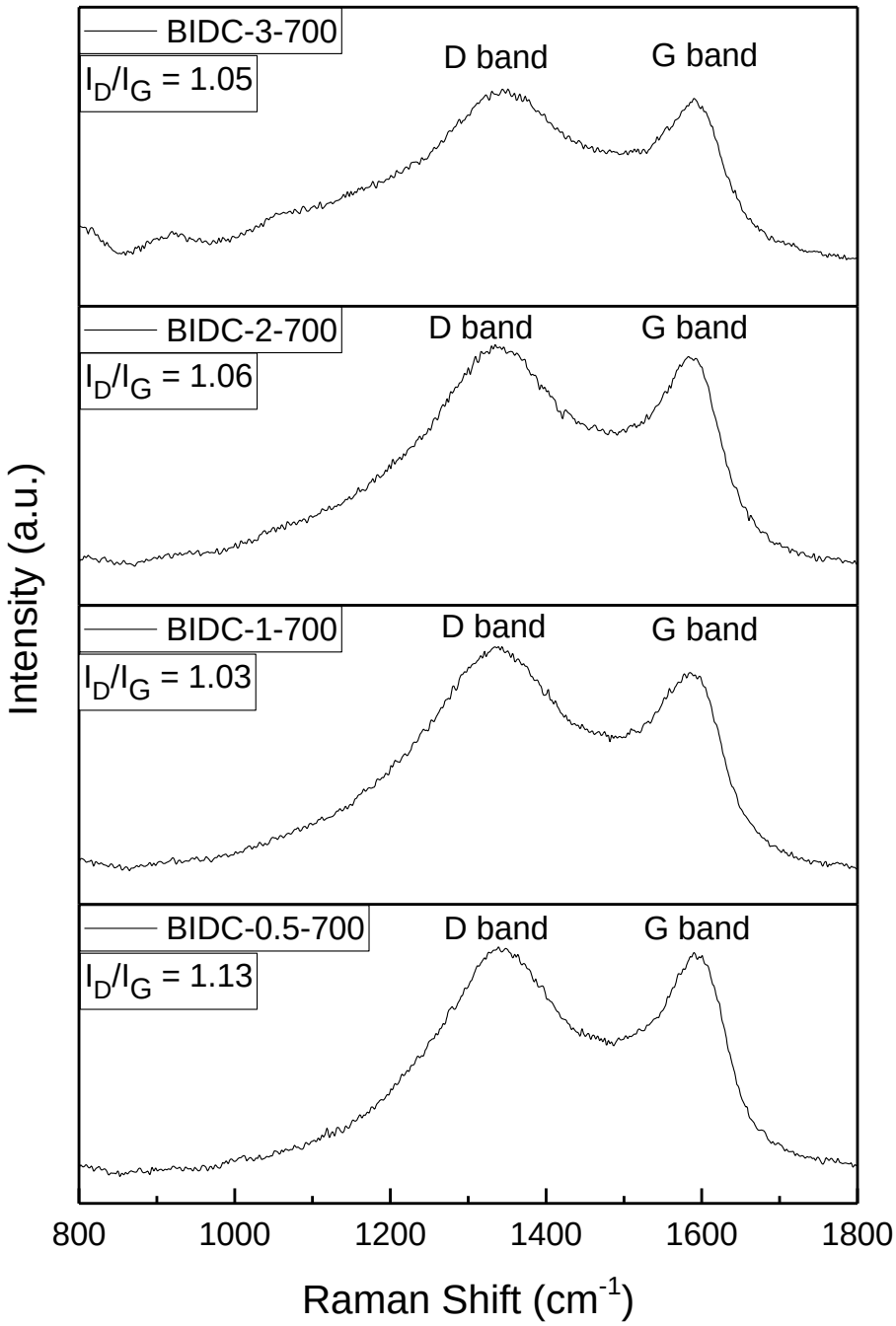

Figure S4. Raman spectra for BIDCs.

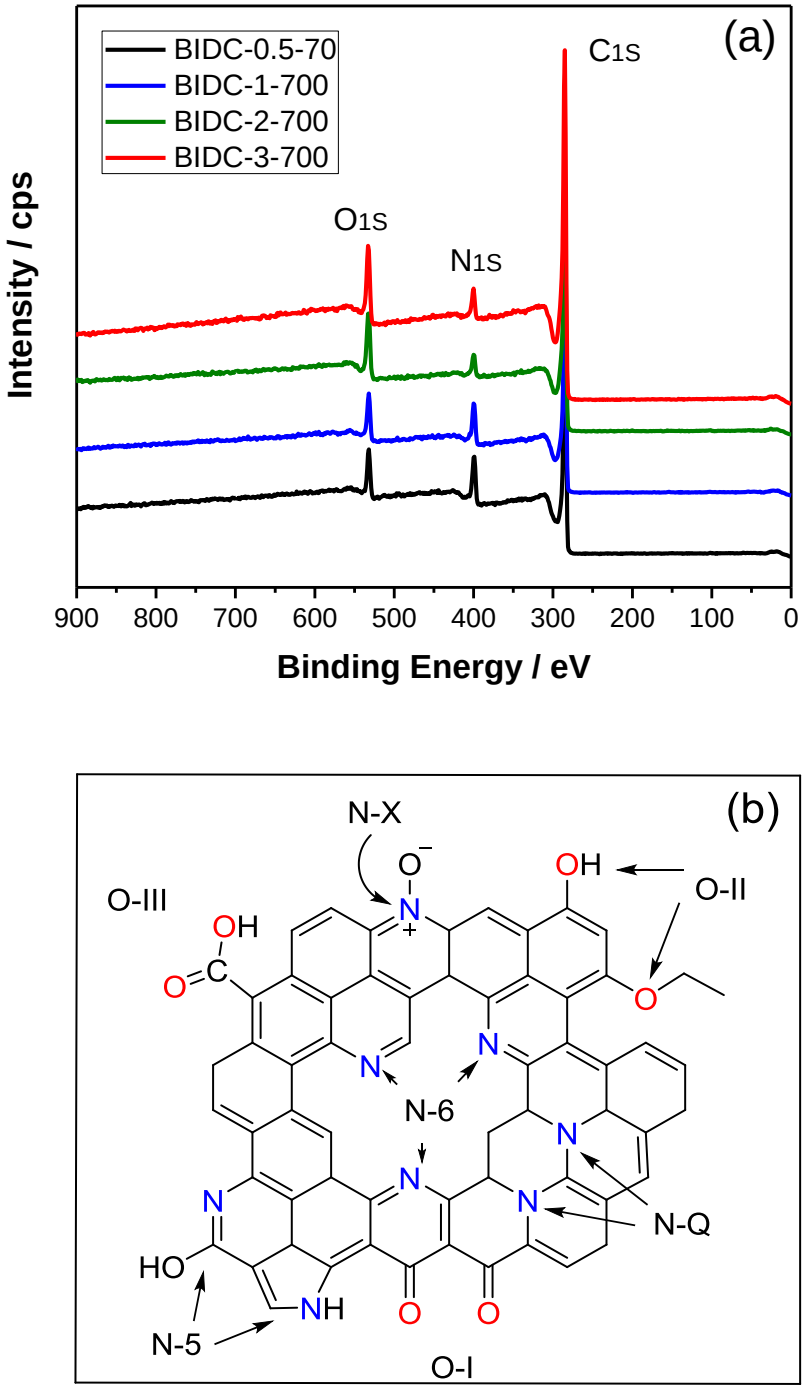

Figure S5. a) X-ray photoelectron spectroscopy (XPS) survey spectra of BIDCs. b) Schematic illustration of various nitrogen and oxygen functionalities on a typical porous carbon.

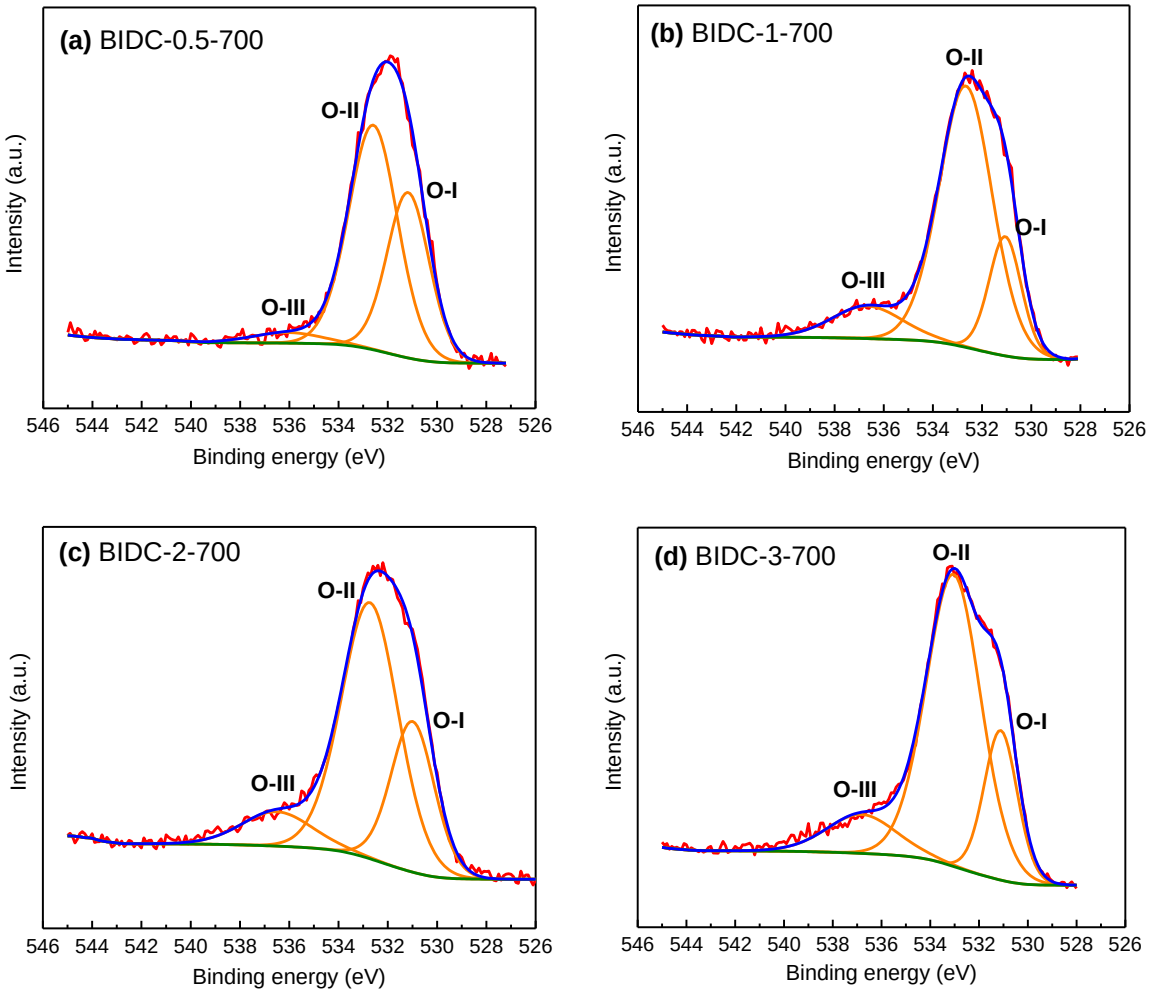

Figure S6. High resolution deconvoluted O 1s spectra for BIDCs. a) BIDC-0.5-700 b) BIDC-1-700 c**)** BIDC-2-700 and d) BIDC-3-700.

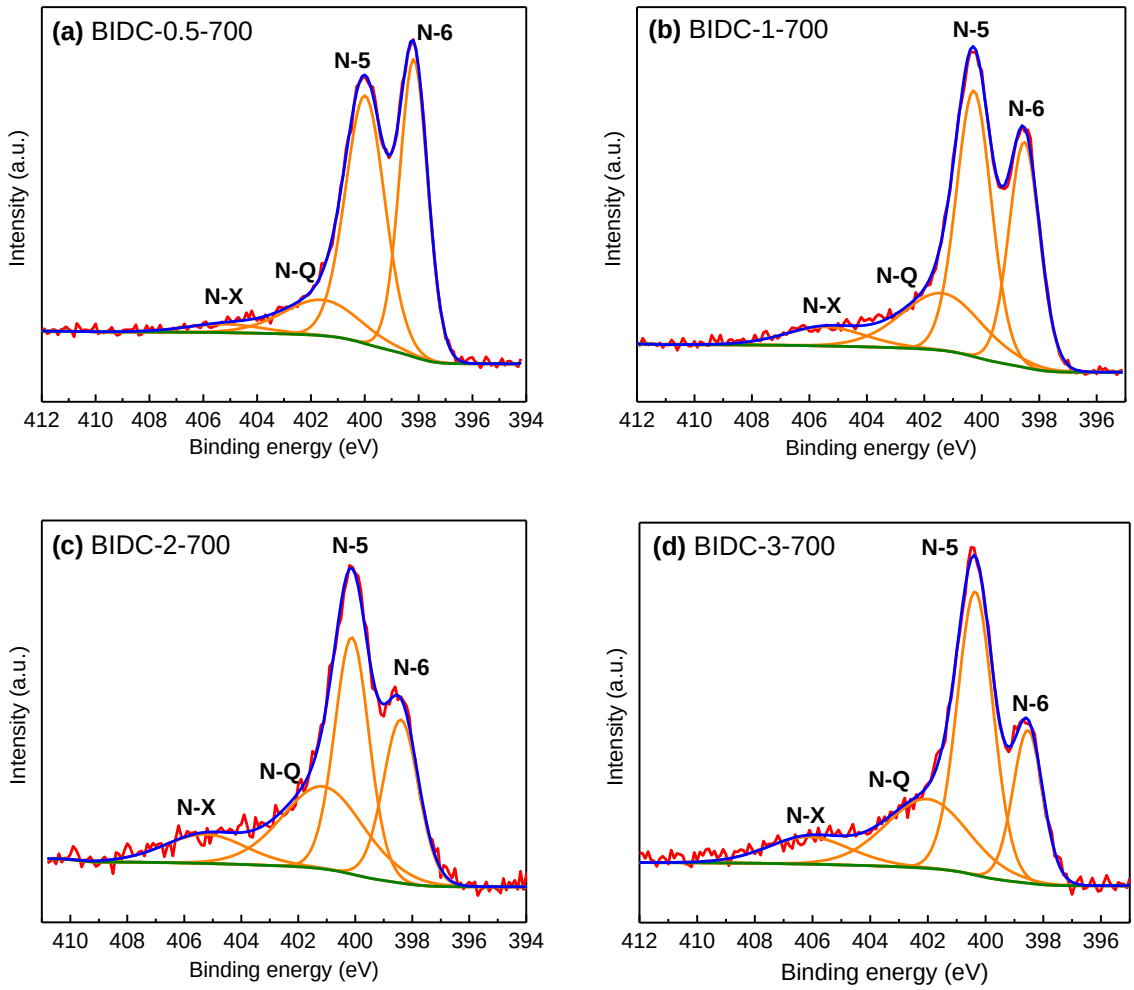

Figure S7. High resolution deconvoluted N 1s spectra for BIDCs. a) BIDC-0.5-700, b) BIDC-1-700, c) BIDC-2-700, and d) BIDC-3-700.

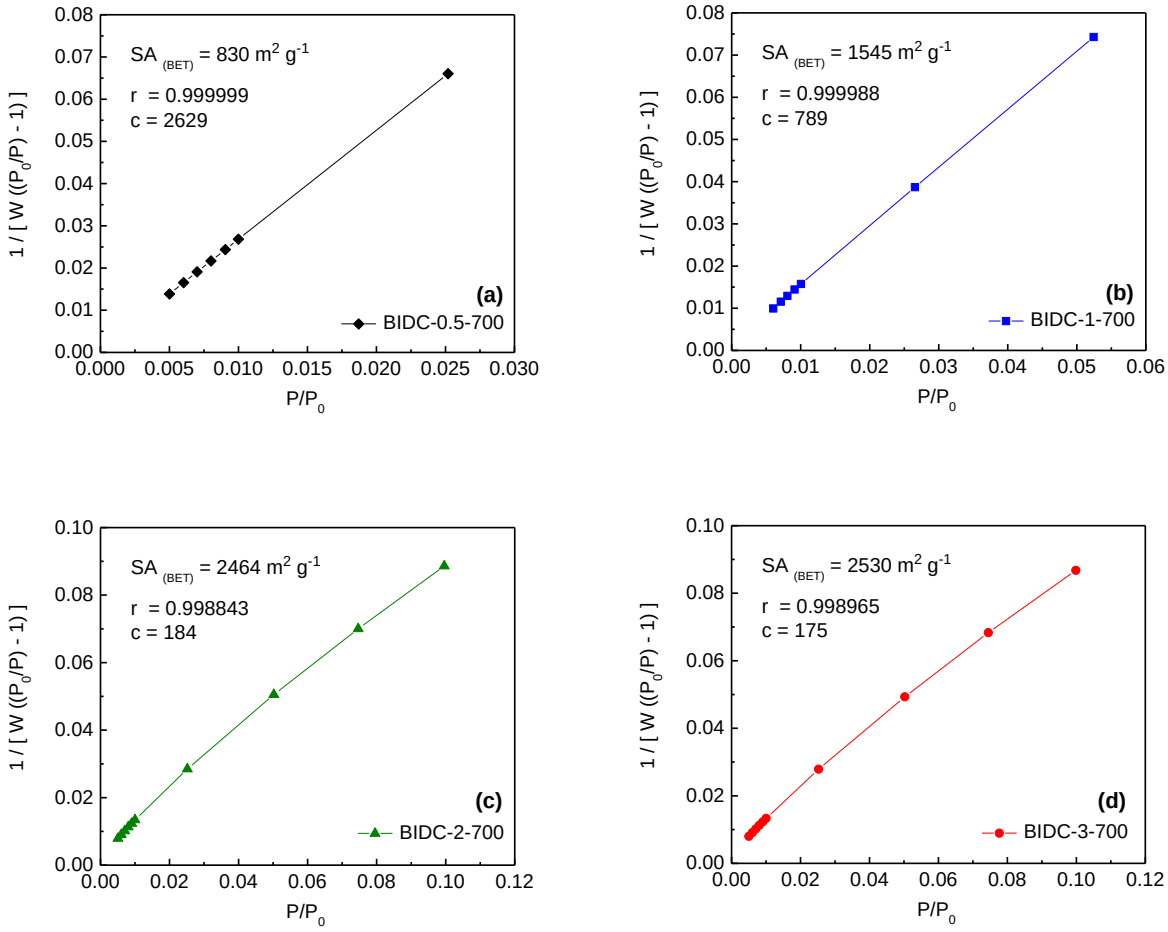

Figure S8. BET plots for BIDCs from the Ar adsorption isotherms at 87 K. a) BIDC-0.5-700 b) BIDC-1-700, c**)** BIDC-2-700, and d) BIDC-3-700. (W = Weight of gas adsorbed at P/P_0, r = Correlation coefficient, c = C constant).

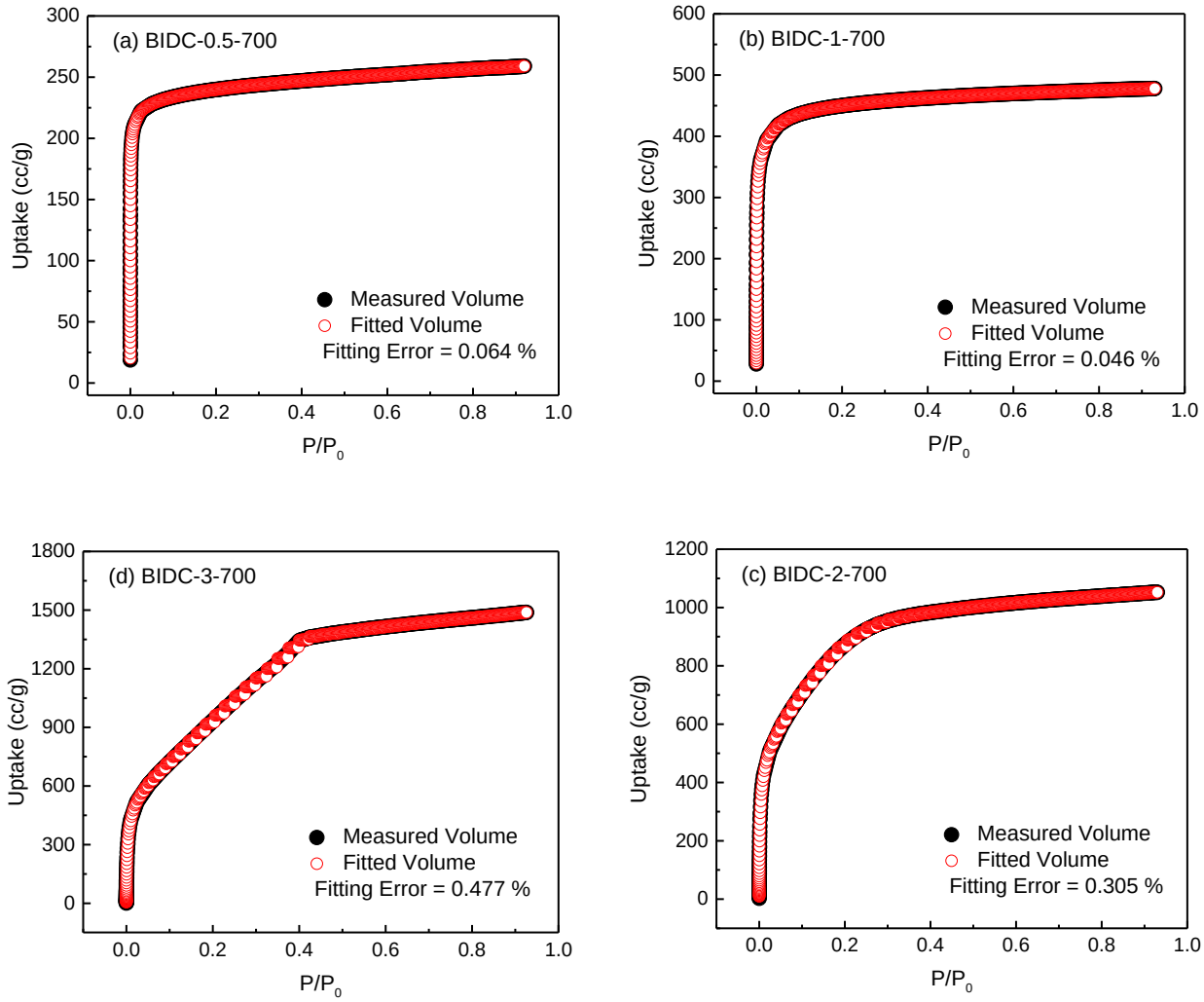

Figure S9. Experimental argon adsorption isotherms (filled black) measured at 87 K and calculated QSDFT isotherms (empty red) for BIDCs.

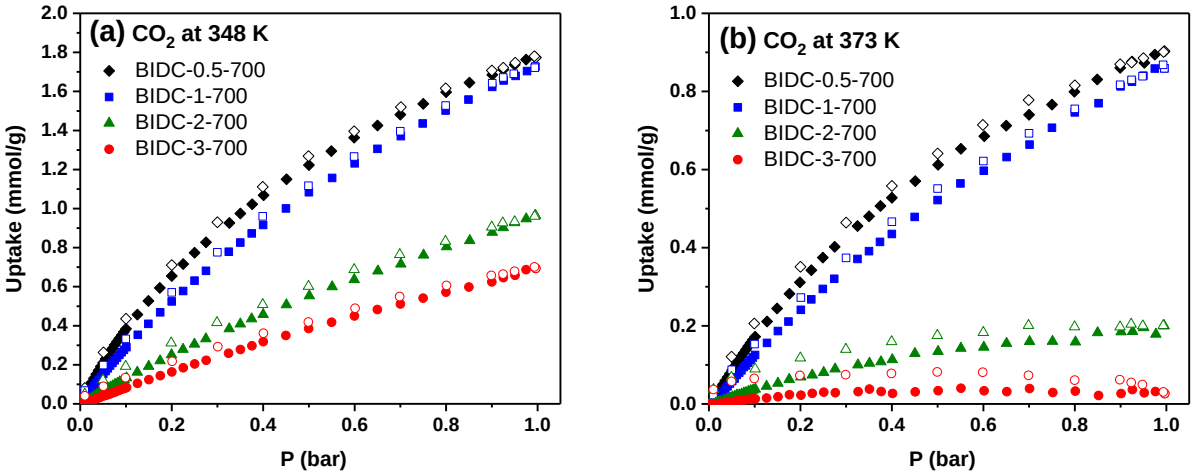

Figure S10. CO_2 isotherms at: a) 348 and b) 373 K for BIDCs.

Table S2. CO_2 uptake values at 348 and 373 K for BIDCs.

	CO_2 capture capacity (mmol g^{-1})			
Carbon	at 0.10 (0.15) bar		at 1 bar	
	348 K	373 K	348 K	373 K
BIDC-0.5-700	0.38 (0.53)	0.17 (0.25)	1.77	0.90
BIDC-1-700	0.29 (0.41)	0.13 (0.19)	1.73	0.86
BIDC-2-700	0.13 (0.19)	0.04 (0.05)	0.97	0.20
BIDC-3-700	0.08 (0.12)	0.01 (0.02)	0.69	0.03

Table S3. CO_2 capture capacity and selectivity values for recently reported porous carbons.

	CO_2 uptake at 298 K (mmol g^{-1})			**Q_{st}**	**N**	**Selectivity at 298 K**		
Adsorbent	1 bar	0.15 bar	0.10 bar		wt%	CO_2/N_2	CO_2/CH_4	
NMC-600	3.90	1.67	-	38	6.3	50[a]	-	ref [1]
SU-MAC-500	4.50	-	1.42	46	5.8	39[a]-124[b]	-	ref [2]
a-NDC-6	4.30	-	1.30*	-	4.8 (at%)	34.23[a]	-	ref [3]
IBN9-NC1-A	4.50	1.75 (0.2 bar)	-	36.1	12.9	27 [b]	-	ref [4]
om-ph-MR	1.77	-	-	32.2	18.2 (at%)	76[a]-100[b]	-	ref [5]
NC700	3.10	1.20*	0.90*	69	20.9	59[a] (273 K)	11[a] (273 K)	ref [6]
CKHP800-2	4.50	1.60	-	29.0	0	43[a]-50[b]	-	ref[7]
MR-1.5-500	3.77	1.29	-	38.5	8.24	43.7[a]-52.9[b]	-	ref[8]
500-2	3.50	-	-	32	11.46	41.6[b]	-	ref[9]
C-600	3.60	1.0	-	43	6.9	33[a]	-	ref[10]
ALPDCK500	3.80	1.50	1.20	37.2	12.1	62[a]	11[a]	ref [11]
CPC-500	5.80	2.10	-	35.3	7.88	65[a]	13[a]	ref [12]
a-MCN	2.69	-	-	38.8	14.45	134[b]	-	ref[13]
BIDC-0.5-700	4.78	2.03	1.60	35.8	17.6	70.4[a]-58.1[b]	13.2[a]-12.4[b]	This work
BIDC-1-700	5.46	1.75	1.32	35.1	13.7	40.9[a]-36.6[b]	8.9[a]-7.4[b]	This work

*) Estimated by extrapolation, a) by initial slope method, b) by IAST method

Table S4. Cumulative ultramicropore volumes for different pore diameters.

	P_V [a)]						
Carbon	d <0.4 nm [$cm^3\ g^{-1}$]	d <0.5 nm [$cm^3\ g^{-1}$]	d <0.6 nm [$cm^3\ g^{-1}$]	d <0.7 nm [$cm^3\ g^{-1}$]	d <0.8 nm [$cm^3\ g^{-1}$]	d<0.9 nm [$cm^3\ g^{-1}$]	d <1.0 nm [$cm^3\ g^{-1}$]
BIDC-0.5-700	0.097	0.178	0.274	0.298	0.308	0.323	0.337
BIDC-1-700	0.071	0.163	0.314	0.372	0.415	0.460	0.489
BIDC-2-700	0.030	0.077	0.195	0.256	0.278	0.342	0.377
BIDC-3-700	0.012	0.051	0.142	0.190	0.233	0.330	0.408

[a)] All data are determined by CO_2 adsorption isotherms (at 273 K) and their derived PSD and cumulative pore volume curves assuming NLDFT and slit shape model

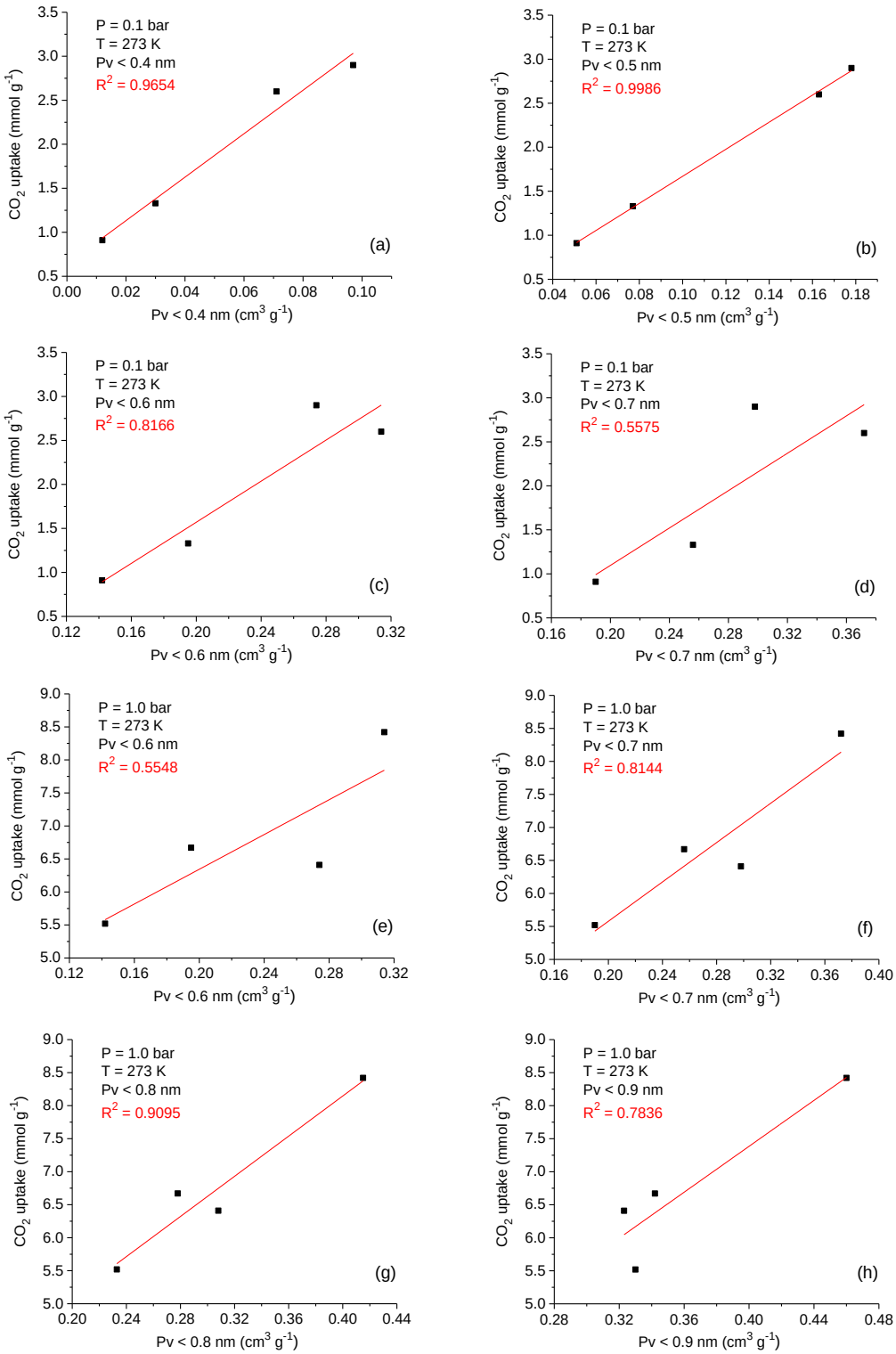

Figure S11. CO_2 uptake at 273 K *versus* volume of ultrafine pores; a-d) at 0.1 bar and e-h) at 1 bar.

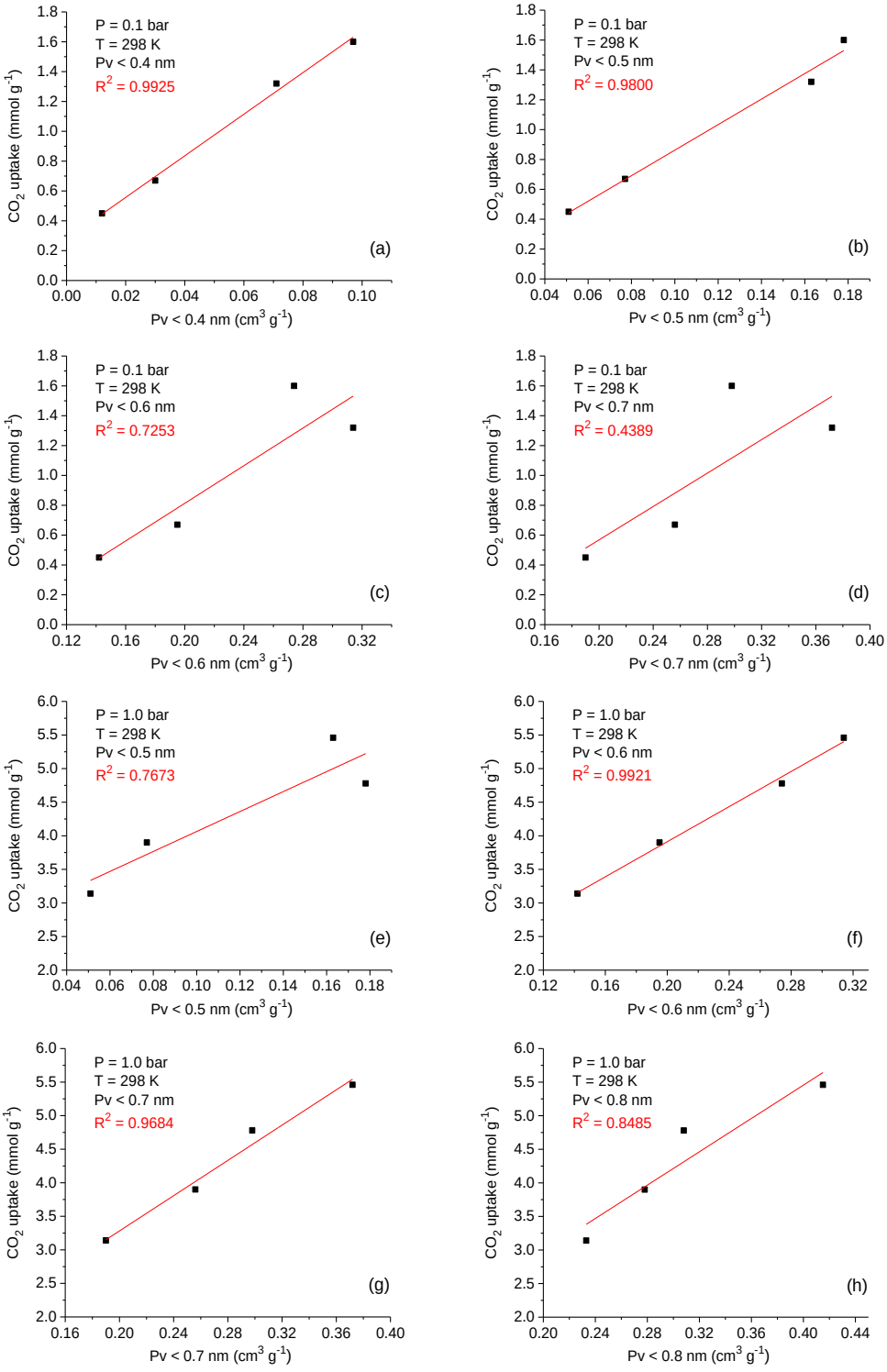

Figure S12. CO_2 uptake at 298 K *versus* volume of ultrafine pores; a-d) at 0.1 bar and e-h) at 1 bar.

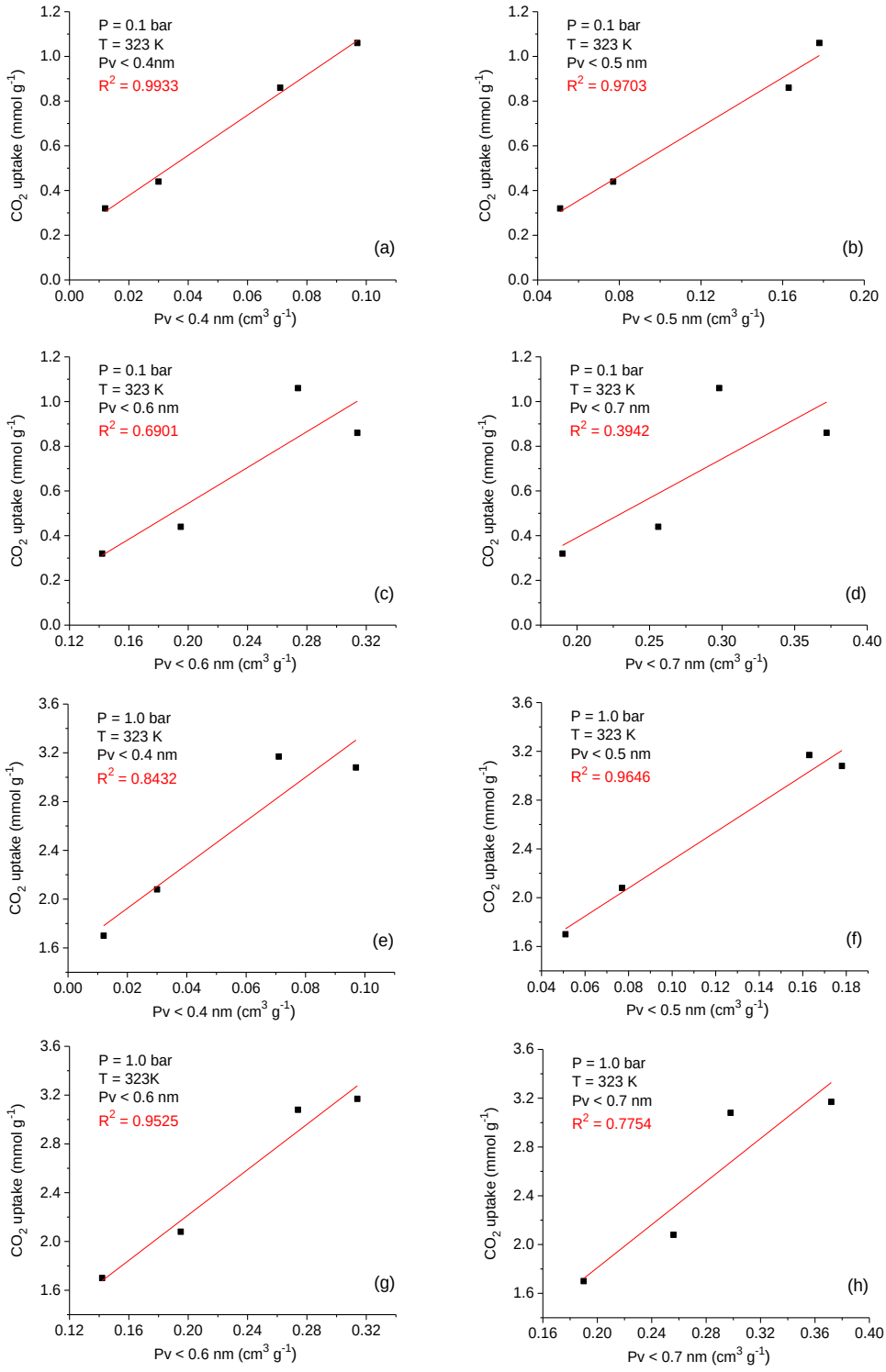

Figure S13. CO_2 uptake at 323 K *versus* volume of ultrafine pores; a-d) at 0.1 bar and e-h) at 1 bar.

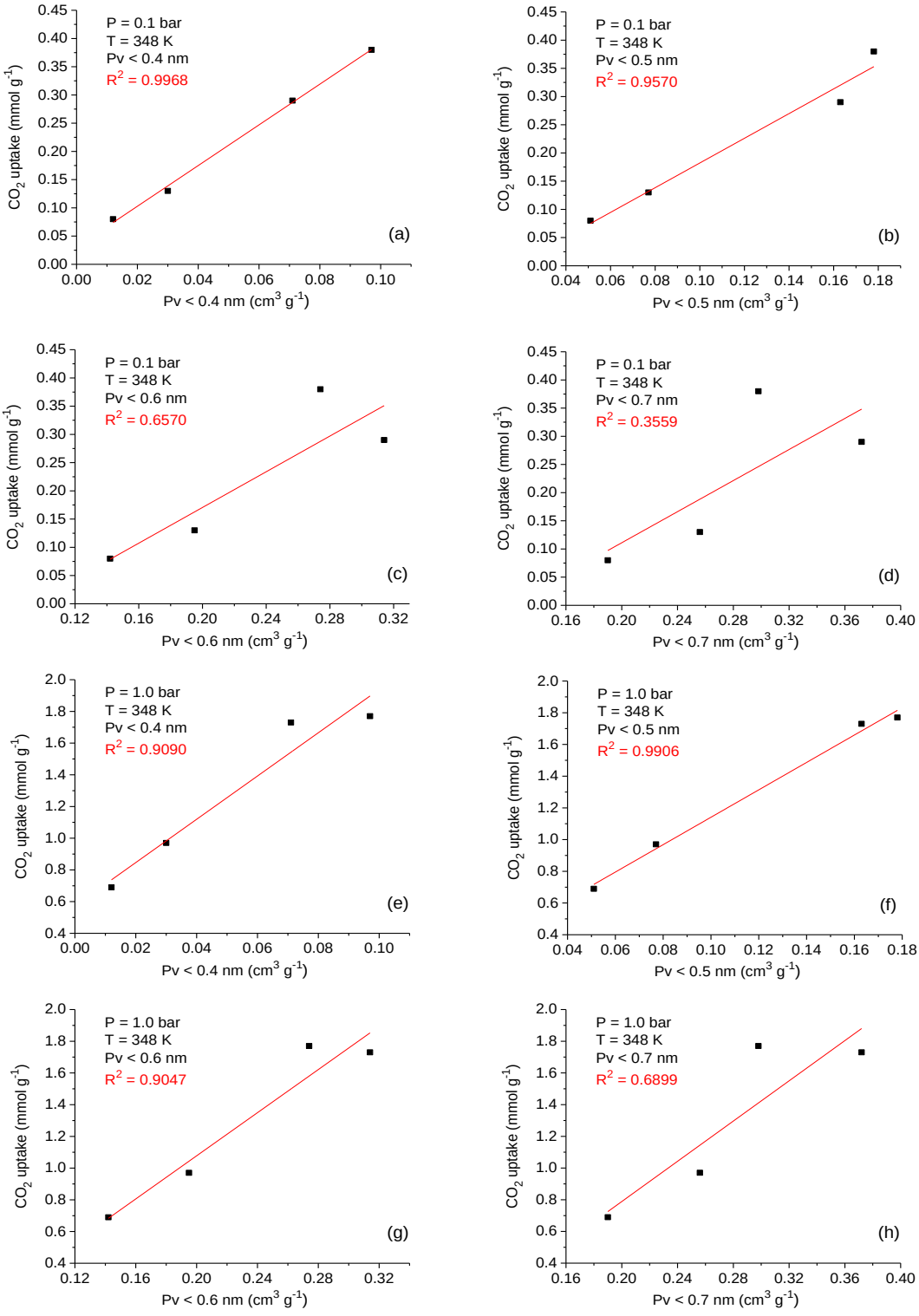

Figure S14. CO_2 uptake at 348 K *versus* volume of ultrafine pores; a-d) at 0.1 bar and e-h) at 1 bar.

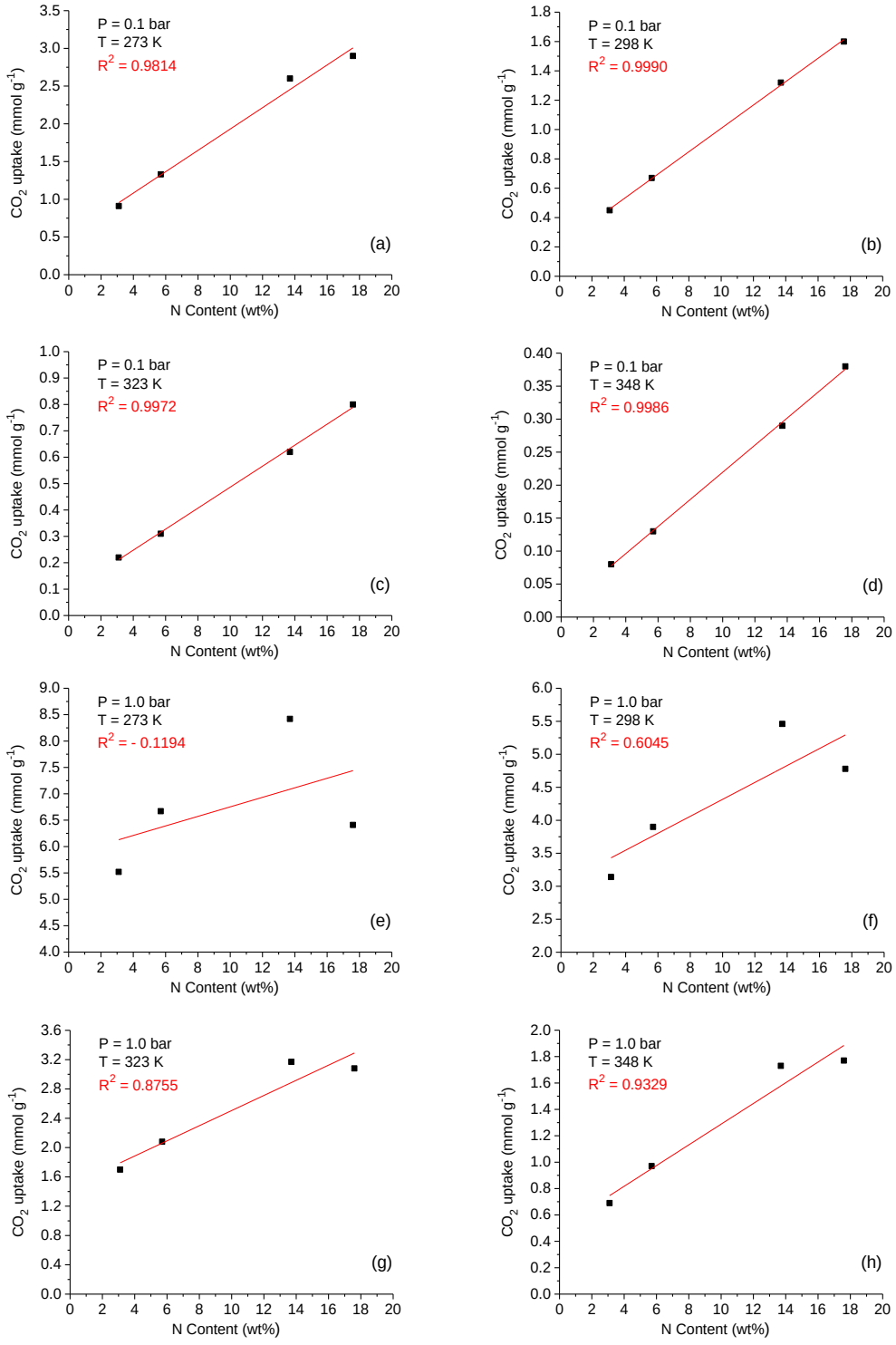

Figure S15. CO_2 uptake *versus* nitrogen content at different temperatures; a-d) at 0.1 bar and e-h) at 1 bar.

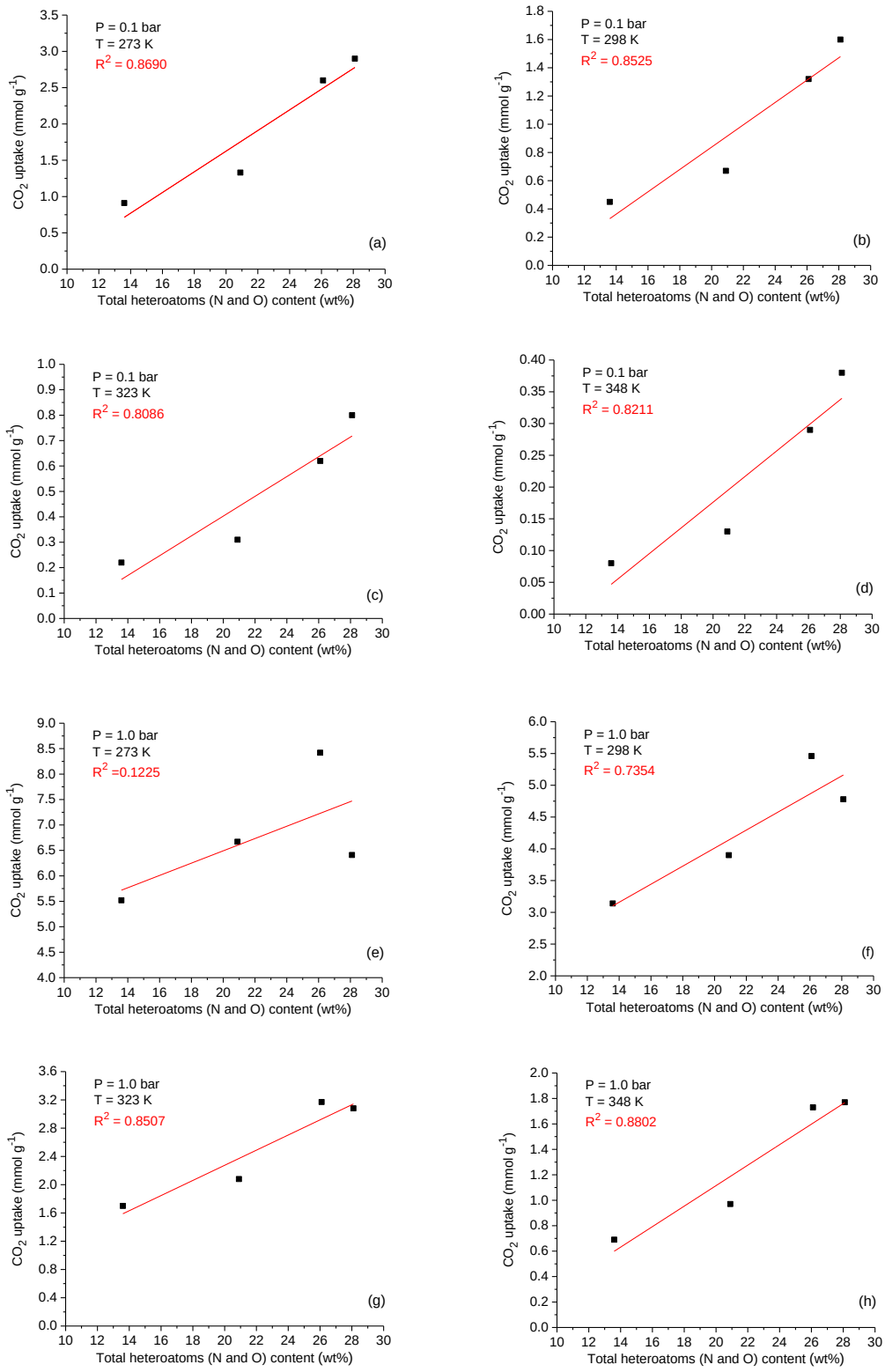

Figure S16. CO_2 uptake *versus* total heteroaotms content at different temperatures; a-d) at 0.1 bar and e-h) at 1 bar.

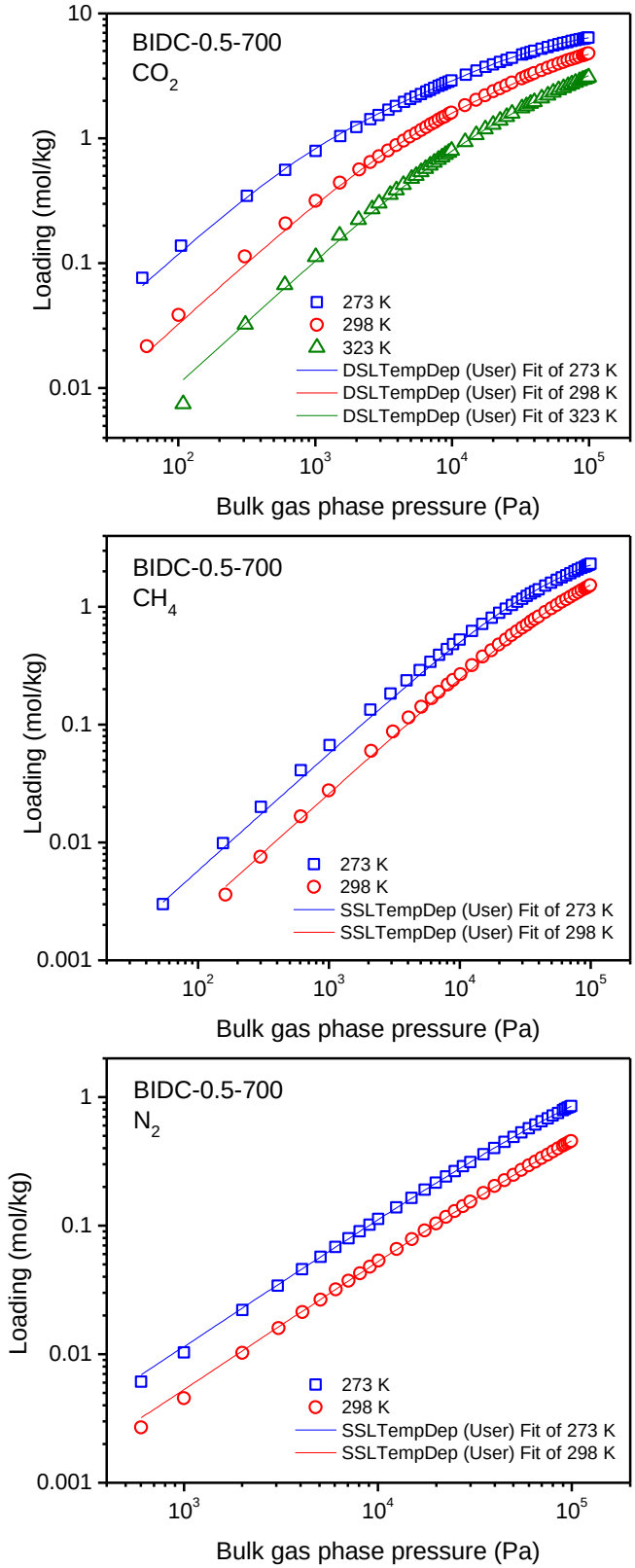

Figure S17. Experimental data and corresponding fittings of gas isotherms for BIDC-0.5-700 (Dual site Langmuir for CO_2, and single site Langmuir for CH_4 and N_2 with temperature dependent parameter).

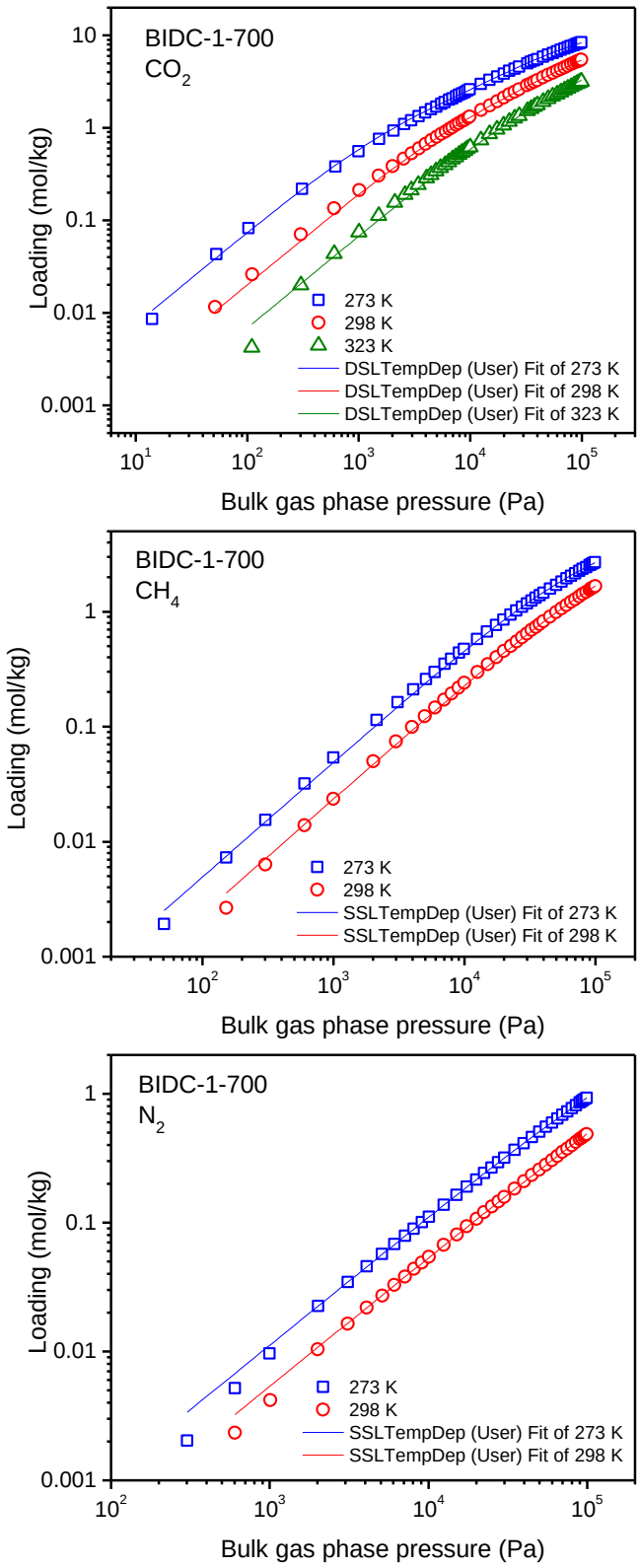

Figure S18. Experimental data and corresponding fittings of gas isotherms for BIDC-1-700 (Dual site Langmuir for CO_2, and single site Langmuir for CH_4 and N_2 with temperature dependent parameter).

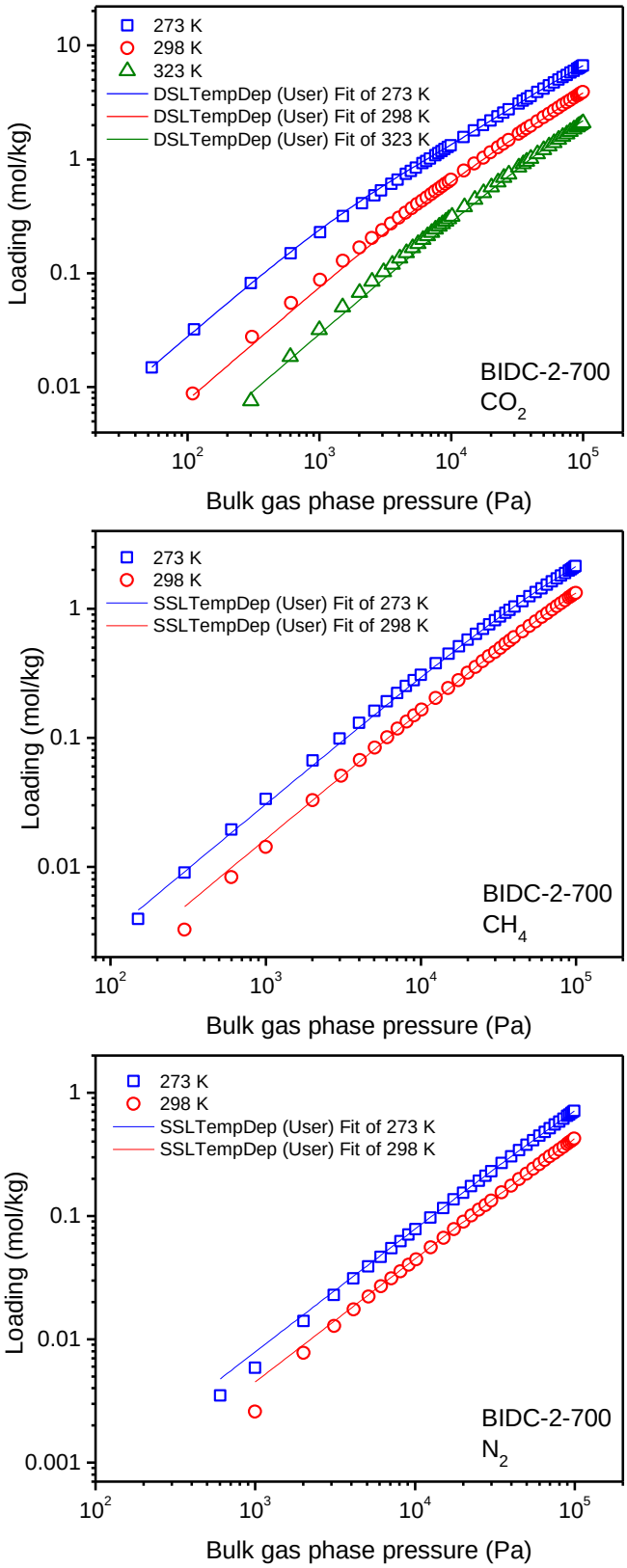

Figure S19. Experimental data and corresponding fittings of gas isotherms for BIDC-2-700 (Dual site Langmuir for CO_2, and single site Langmuir for CH_4 and N_2 with temperature dependent parameter).

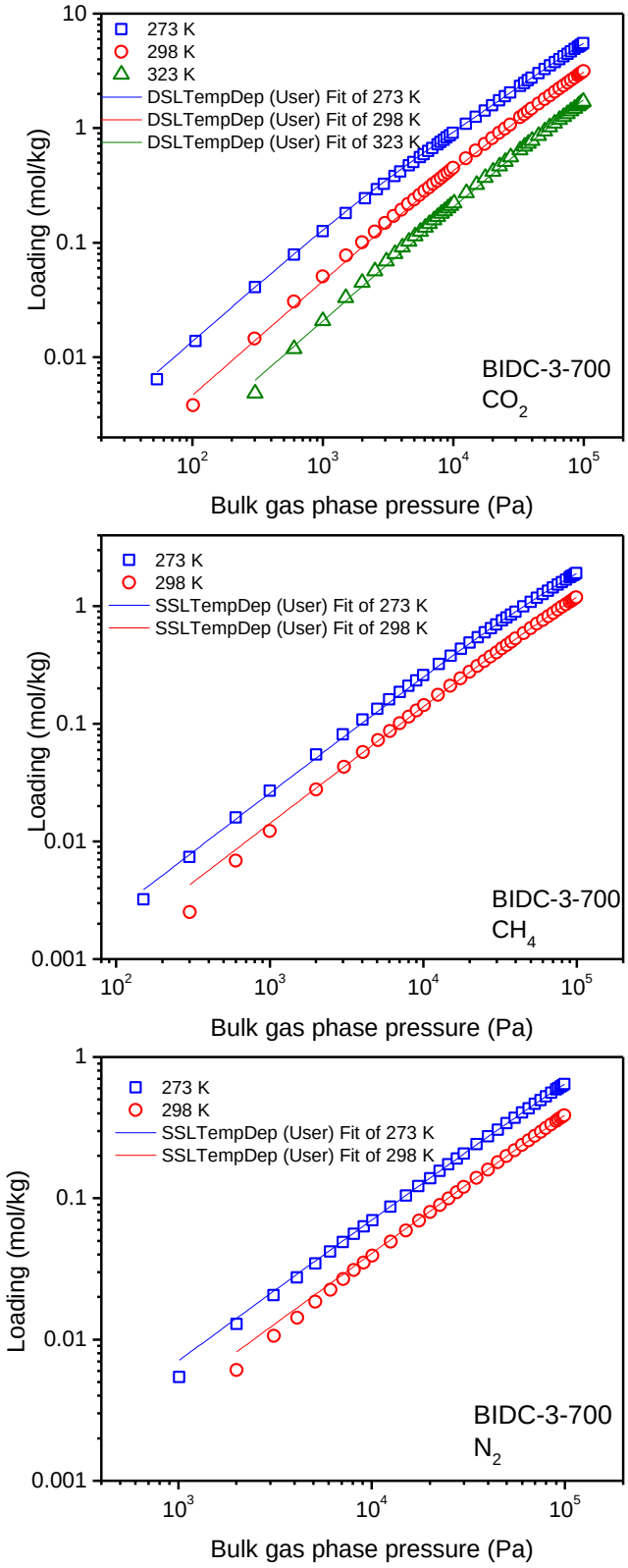

Figure S20. Experimental data and corresponding fittings of gas isotherms for BIDC-3-700 (Dual site Langmuir for CO_2, and single site Langmuir for CH_4 and N_2 with temperature dependent parameter).

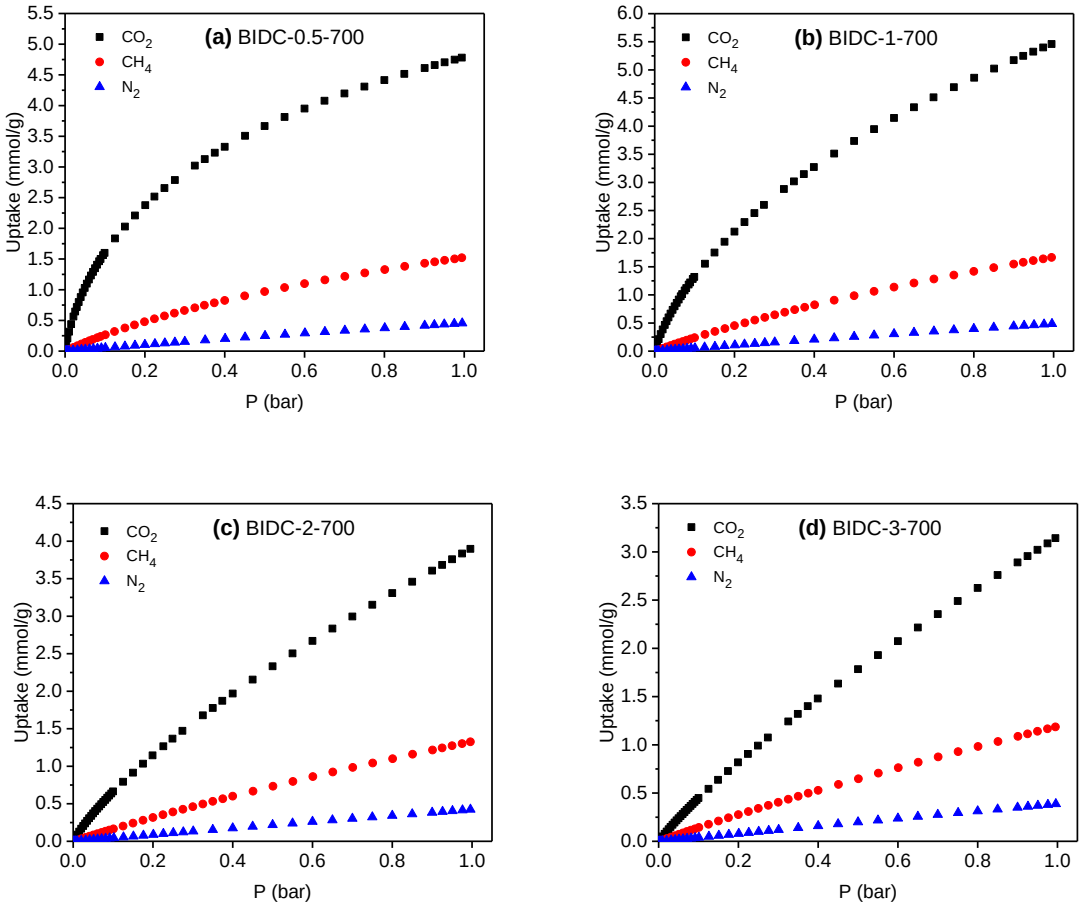

Figure S21. Experimental pure component curves at 298 K for: a) BIDC-0.5-700, b) BIDC-1-700, c) BIDC-2-700 and d) BIDC-3-700.

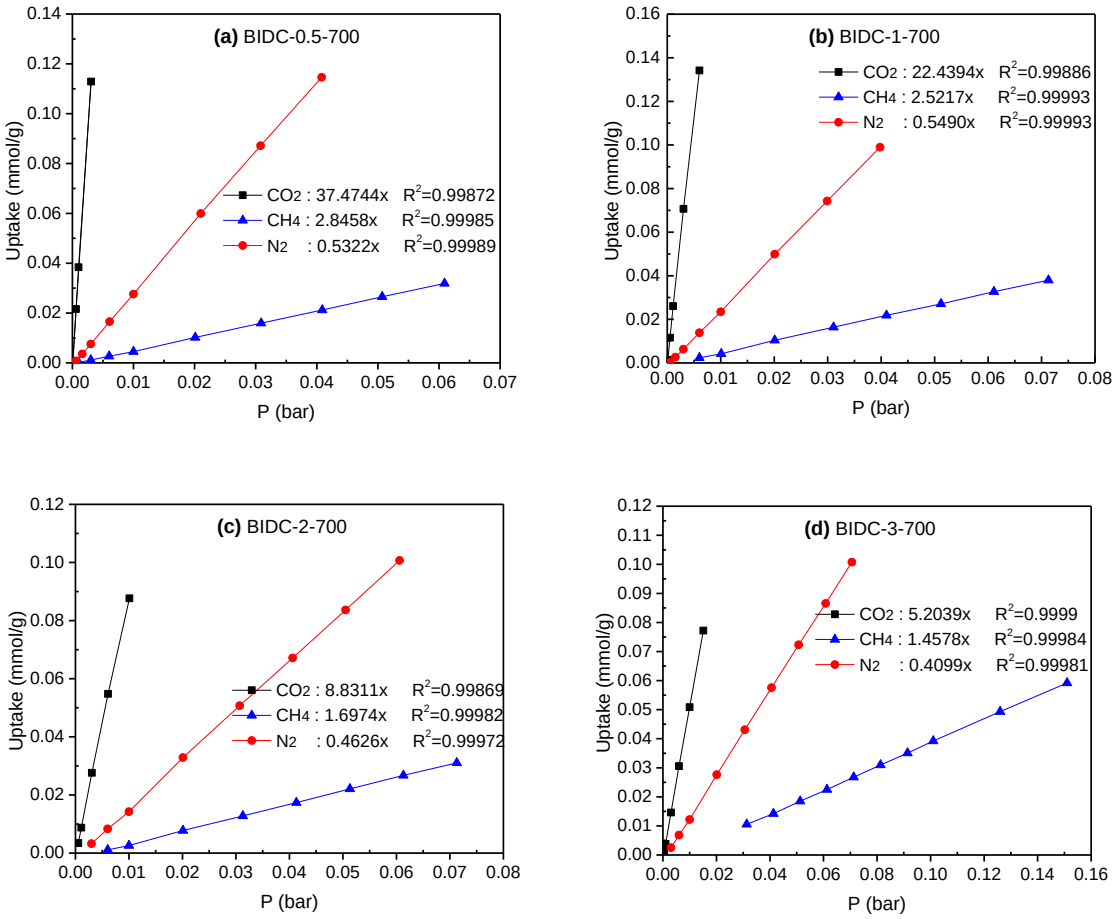

Figure S22. CO_2/N_2 and CO_2/CH_4 adsorption selectivity at 298 K for: a) BIDC-0.5-700, b) BIDC-1-700, c) BIDC-2-700, and d) BIDC-3-700.

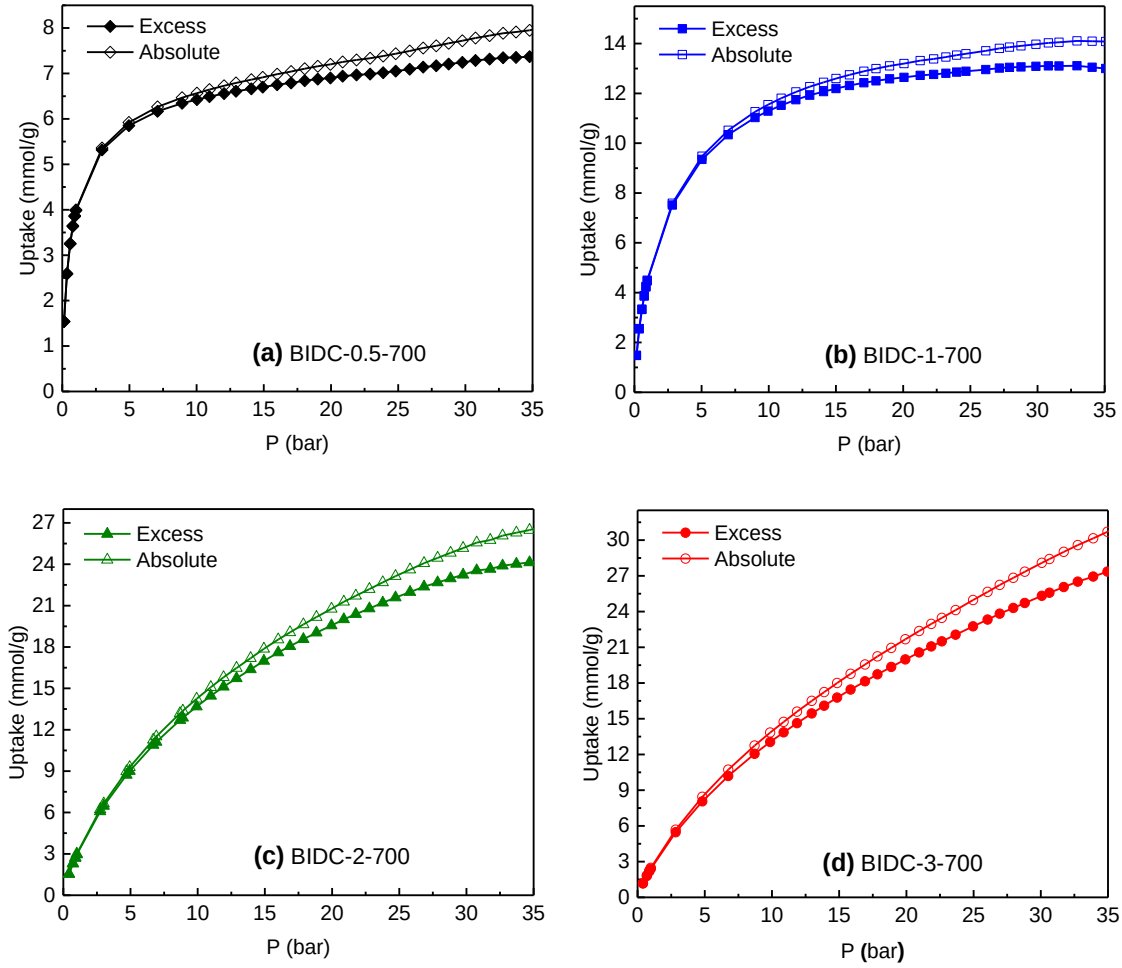

Figure S23. Comparison of CO_2 surface excess and absolute uptakes for BIDCs.

Table S5. Cumulative volumes for large micropores and narrow mesopores.

	CO_2 uptake at 30 bar and 298 K		P_V [a)]			
Carbons	Excess [mmol g^{-1}]	Absolute [mmol g^{-1}]	d<1.5 nm [cm^3 g^{-1}]	d<2.0 nm [cm^3 g^{-1}]	d<2.2 nm [cm^3 g^{-1}]	d<2.4 nm [cm^3 g^{-1}]
BIDC-0.5-700	7.3	7.7	0.305	0.308	0.309	0.310
BIDC-1-700	13.1	14.0	0.579	0.586	0.587	0.588
BIDC-2-700	23.4	25.3	0.810	1.157	1.211	1.235
BIDC-3-700	25.3	28.1	0.654	1.121	1.296	1.464

[a)] Pore volumes are determined by Ar adsorption isotherms (at 87 K) and their derived PSD and cumulative pore volume curves assuming QSDFT and slit shape model.

The *absolute* adsorption values (void space of the pores of adsorbent can hold significant amount of compressed gas under high pressures) were estimated from the well-established [14] Equation S1 as below:

$$N_{abs} = N_{exc} + \rho_{gas} V_p \quad \text{(S1)}$$

Where N_{abs} is the absolute adsorption, N_{exc} is the excess adsorption measured experimentally, ρ_{gas} is the density of the compressed gas at a given temperature and pressure (determined using NIST Thermochemical Properties of Fluid Systems)[15] and V_p is the total pore volume obtained from the Ar isotherm at 87 K.

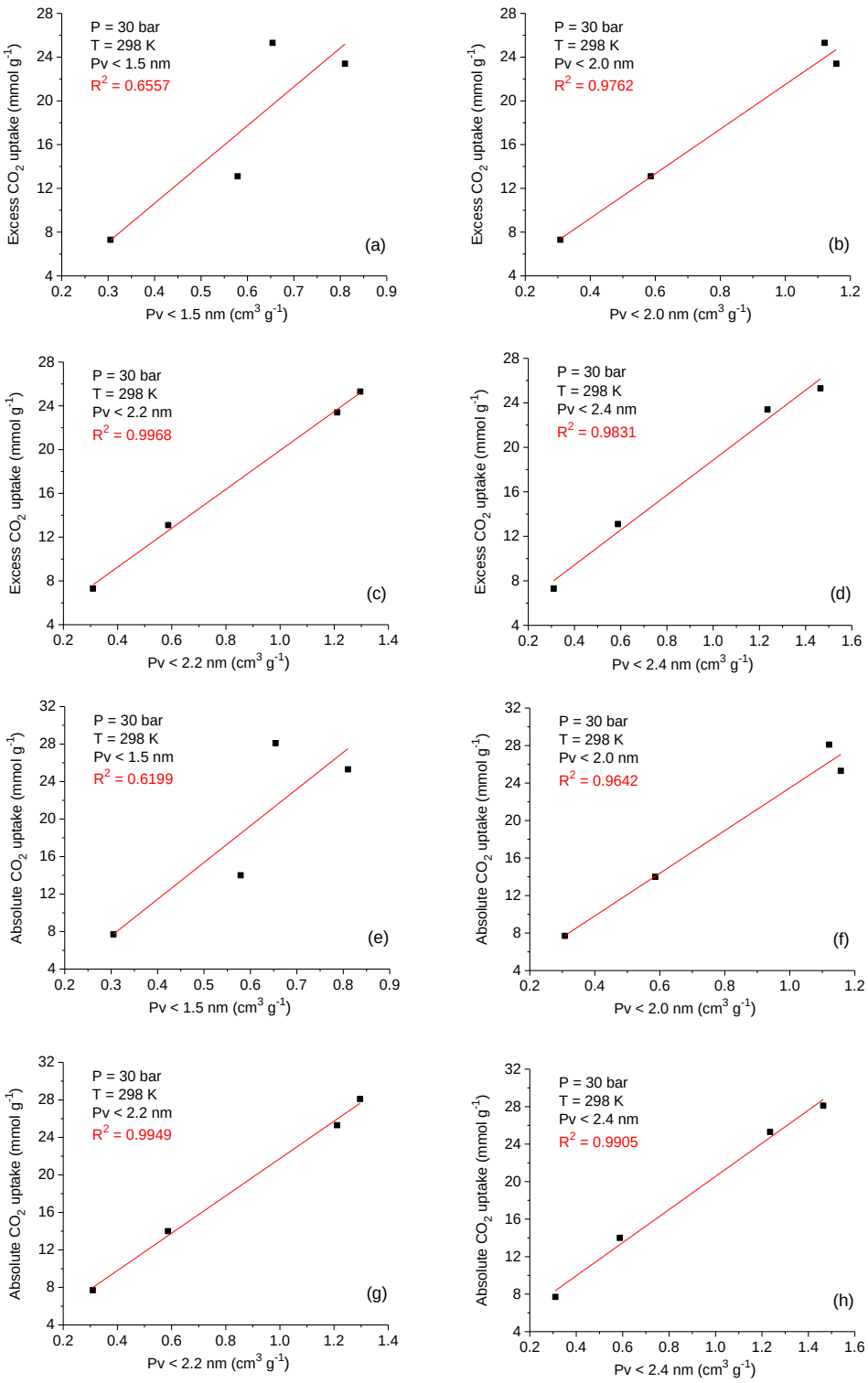

Figure S24. CO_2 uptake at 298 K *versus* volume of large micropores and narrow mesopores; a-d) surface excess uptake and e-h) absolute uptake.

Selectivity and heat of adsorption calculation. The pure component isotherms of CO_2 measured at 273, 298 and 323 K were fitted with the dual-site Langmuir (DSL) model, which is calculated by the Equation S2:

$$q = q_A + q_B = q_{sat,A}\frac{b_A p}{1 + b_A p} + q_{sat,B}\frac{b_B p}{1 + b_B p} \quad \text{(S2)}$$

with T-dependent parameters b_A and b_B being defined as Equation S3 and S4:

$$b_A = b_{A0}\, exp\left(\frac{-E_A}{RT}\right) \quad \text{(S3)}$$

$$b_B = b_{B0}\, exp\left(\frac{-E_B}{RT}\right) \quad \text{(S4)}$$

where, q is molar loading of adsorbate (mol kg^{-1}), q_{sat} is saturation loading (mol kg^{-1}) , b is a parameter in the pure component Langmuir isotherm (Pa^{-1}), ρ is bulk gas phase pressure (Pa), $-E$ is heat of adsorption (J mol^{-1}), R is the ideal gas constant (8.314 J mol^{-1} K^{-1}), T is absolute temperature (K), and subscripts A and B refer to site A and site B, respectively.

Since the pure component isotherms of CH_4 and N_2 do not show any inflection characteristic, they were fitted with the single-site Langmuir (SSL) model, which uses Equation S5:

$$q = q_{sat,A}\frac{b_A p}{1+b_A p} \quad \text{(S5)}$$

with the T-dependent parameter b_A defined by Equation S3.

Pure-component isotherm fitting parameters were then used for calculating the Ideal Adsorbed Solution Theory (IAST) binary-gas adsorption selectivities, S_{ads}, which are calculated as Equation S6:

$$S_{ads} = \frac{q_1/q_2}{p_1/p_2} \quad \text{(S6)}$$

CO_2 fitting parameters also were used to calculate the isosteric heats of adsorption (Q_{st}) using the Clausius-Clapeyron equation as below:

$$(\ln P)_n = \left(\frac{Q_{st}}{R}\right)\left(\frac{1}{T}\right) + C \quad \text{(S7)}$$

where, P is the pressure, n is the amount adsorbed, T is the temperature, R is the universal gas constant, and C is the equation constant. The isosteric heat of adsorption was obtained from the slope of plots of ln P as a function of 1/T.

References

[1] J. Zhou, Z. Li, W. Xing, T. Zhu, H. Shen, S. Zhuo, *Chem. Commun.* **2015**, *51*, 4591.

[2] J. W. F. To, J. He, J. Mei, R. Haghpanah, Z. Chen, T. Kurosawa, S. Chen, W.-G. Bae, L. Pan, J. B. H. Tok, J. Wilcox, Z. Bao, *J. Am. Chem. Soc.* **2016**, *138*, 1001.

[3] V. Chandra, S. U. Yu, S. H. Kim, Y. S. Yoon, D. Y. Kim, A. H. Kwon, M. Meyyappan, K. S. Kim, *Chem. Commun.* **2012**, *48*, 735.

[4] Y. Zhao, L. Zhao, K. X. Yao, Y. Yang, Q. Zhang, Y. Han, *J. Mater. Chem.* **2012**, *22*, 19726.

[5] J. H. Lee, H. J. Lee, S. Y. Lim, B. G. Kim, J. W. Choi, *J. Am. Chem. Soc.* **2015**, *137*, 7210.

[6] A. Aijaz, N. Fujiwara, Q. Xu, *J. Am. Chem. Soc.* **2014**, *136*, 6790.

[7] B. Adeniran, E. Masika, R. Mokaya, *J. Mater. Chem. A* **2014**, *2*, 14696.

[8] H. Cong, M. Zhang, Y. Chen, K. Chen, Y. Hao, Y. Zhao, L. Feng, *Carbon* **2015**, *92*, 297.

[9] D. Lee, C. Zhang, C. Wei, B. L. Ashfeld, H. Gao, *J. Mater. Chem. A* **2013**, *1*, 14862.

[10] X. Zhang, D. Lin, W. Chen, *RSC Adv.* **2015**, *5*, 45136.

[11] B. Ashourirad, P. Arab, A. Verlander, H. M. El-Kaderi, *ACS Appl. Mater. Interfaces* **2016**, *8*, 8491.

[12] B. Ashourirad, A. K. Sekizkardes, S. Altarawneh, H. M. El-Kaderi, *Chem. Mater.* **2015**, *27*, 1349.

[13] D. Li, Y. Chen, M. Zheng, H. Zhao, Y. Zhao, Z. Sun, *ACS Sustainable Chem. Eng.* **2016**, *4*, 298.

[14] M. E. Casco, M. Martínez-Escandell, E. Gadea-Ramos, K. Kaneko, J. Silvestre-Albero, F. Rodríguez-Reinoso, *Chem. Mater.* **2015**, *27*, 959.

[15] NIST Chemistry WebBook (Thermophysical Properties of Fluid Systems). http://webbook.nist.gov/chemistry/fluid/.